

# REVIEWS OF MODERN PHYSICS

VOLUME 44, NUMBER 1

JANUARY 1972

## Energy Spectra of Electrons Ejected in Ion-Atom Collisions

GENNADI N. OGURTSOV

*A. F. Ioffe Physico-Technical Institute, USSR Academy of Sciences, Leningrad, USSR.*

The available experimental data on energy spectra of electrons ejected in ion-atom collisions are reviewed against the background of modern theoretical concepts.

### CONTENTS

|   |    |
|---|----|
| Introduction.....                                     | 1  |
| 1. Theoretical background.....                        | 2  |
| A. Born approximation.....                            | 2  |
| B. Classical binary-encounter approximation.....      | 2  |
| C. Statistical models.....                            | 3  |
| D. Autoionization.....                                | 4  |
| E. Molecular orbital theory.....                      | 6  |
| 2. Experimental results and discussion.....           | 7  |
| A. Experimental technique.....                        | 8  |
| B. Collisions between two light atomic particles..... | 8  |
| C. Collisions between protons and heavy atoms.....    | 10 |
| D. Collisions between two heavy atomic particles..... | 12 |
| Conclusions.....                                      | 16 |
| Acknowledgments.....                                  | 16 |
| References.....                                       | 16 |

### INTRODUCTION

The investigations which will be considered in this article represent one of the trends in studying ionization processes in atomic collisions.

Ionization is always accompanied by a change in some of the parameters characterizing the states of colliding particles, namely:

- (a) a change in charge of the incident particle and target atom,
- (b) a change in kinetic energy of the particles involved in the collision,
- (c) a change in directions of the colliding particles,
- (d) ejection of electrons distributed in a certain way in kinetic energy and ejection angle.

Historically, it is the first three parameters that have remained the major subject of experimental and theoretical study. In investigations of the ejected electrons, the efforts of experimentalists have been aimed only at

measuring the total ionization cross sections. It was not until recently that a systematic and intensive study of electron energy and angular distribution was initiated.

The first experimental results on energy spectra of electrons ejected in ion-atom collisions were obtained in 1957 by Blauth (B157) who studied collisions between protons and gas atoms and molecules in the proton energy range 12–50 keV. It was found that the electron energy distribution was represented by a smooth curve diminishing with increasing electron energy, and extending up to energies of about several hundred electronvolts. In some cases diffuse maxima were observed in the distribution. However, this structure was obscured, since the energy interval between two successive experimental points in (B157) was much larger than that defined by the energy resolution of the analyzer.

Subsequently, the investigations of electron energy spectra were continued by Moe and Petsch (MP58,59) who studied collisions between potassium ions and noble gas atoms. These authors found a distinct structure in the energy spectra which was characteristic of the particular gas atom. The results obtained in (MP58,59) provided the first experimental evidence for autoionization state excitation in ion-atom collisions. A similar structure in electron energy spectra was observed by Berry (B61,62; BB66) in experiments on collisions between ions and atoms of noble gases.

In recent years the study of electron energy spectra has been considerably stimulated by the appearance of new data (AGPF64; EK65) on inelastic energy losses in ion-atom collisions. A discrete structure in inelastic energy loss spectra observed at the values of energy

losses above the ionization energy indicated the possibility of de-excitation via autoionization processes. In fact, the recent experiments (RJV66; CJ70; OFAF68; OFA70; O71) on electron energy spectra reveal a close correlation between the structure in the inelastic energy loss spectrum and the peculiarities of electron energy distribution caused by autoionization transitions in the colliding particles. This correlation was established directly in experiments on coincidences between scattered ions and electrons ejected in  $\text{Ar}^+-\text{Ar}$  collisions (TLE70).

At present, the investigation of the electron energy spectra has become an important method for studying the mechanism of inelastic atomic collisions. The body of experimental data accumulated during the past decade exceeds the limits of a single article. Therefore, we shall restrict ourselves to the discussion of those results which we think reflect the most essential features of electron energy spectra, and are of interest to the theoretical study of the mechanism of inelastic atomic collisions. Most attention will be given to the ionization processes occurring at energies of relative motion of the order of  $10^4-10^5$  eV.

## 1. THEORETICAL BACKGROUND

This section will be devoted to the description of the theoretical models and calculations used in interpretation of experimental data on electron energy spectra. It is not aimed at a detailed consideration of the problems and is addressed to experimentalists rather than to theoreticians. The latter, we hope, will realize how modest are the theoretical achievements in this field of the physics of atomic collisions.

### A. Born Approximation

The theoretical study of energy distribution of electrons ejected in ion-atom collisions was initiated in 1953 by Bates and Griffing (BG53) (cf., Be33) who calculated cross sections for excitation and ionization of hydrogen atoms bombarded by fast protons and hydrogen atoms, using the first Born approximation. The energy distribution of ejected electrons was obtained in the course of the calculation of the total ionization cross section

$$d^2\sigma/d\Omega d\kappa = (4z^2e^4/\hbar^2v^2) \times \iint |\int \Psi_{\kappa}^{(-)*} \exp(-i\mathbf{q}\mathbf{r}) \Psi_0 \mathbf{r} |^2 (dq/q^3) d\varphi, \quad (1)$$

where  $ze$  is the incident ion charge,  $v$  is the ion velocity,  $\mathbf{r}$  is the electron radius,  $q = (1/\hbar) |\mathbf{K} - \mathbf{K}'|$  is the transferred momentum,  $\mathbf{K}$  and  $\mathbf{K}'$  are the ion momenta before and after the collision respectively,  $\Psi_0$  and  $\Psi_{\kappa}^{(-)}$  are the initial and final state wave functions,  $\kappa^2$  is the kinetic energy of the ejected electron in Rydbergs,  $\Omega$  is the ejection solid angle, and  $\varphi$  is the ion azimuth angle.

The integration over the coordinate  $\mathbf{r}$  and  $\varphi$  can be

made analytically and yields

$$\frac{d^2\sigma}{d\Omega d(\kappa^2)} = \int_{q_{\min}}^{q_{\max}} \frac{\exp\{- (2/\kappa) \arctan [2\kappa/(q^2 - \kappa^2 + 1)]\} (dq/q)}{[(q+\kappa)^2 + 1][(q-\kappa)^2 + 1][1 - \exp(-2\pi/\kappa)]} \times \frac{2AD^3 + 3AD\epsilon^2 - 4BD^2\epsilon - B\epsilon^3 + CD^3 + 4CD\epsilon^2}{(D^2 - \epsilon^2)^{7/2}}, \quad (2)$$

$$A = q^2 - 2q_{\min}\kappa \cos\theta + (\kappa^2 + 1)(q_{\min}^2/q^2) \cos^2\theta,$$

$$B = [2(q^2 - q_{\min}^2)^{1/2}/q^2] \sin\theta [\kappa q^2 - q_{\min} \cos\theta(\kappa^2 + 1)],$$

$$C = (\kappa^2 + 1) \{ [(q^2 - q_{\min}^2)/q^2] \sin^2\theta \},$$

$$D = q^2 - 2q_{\min}\kappa \cos\theta + \kappa^2 + 1,$$

$$\epsilon = 2\kappa(q^2 - q_{\min}^2)^{1/2} \sin\theta,$$

$$q_{\min} = (\Delta E/\hbar v) [1 + (\Delta E/2Mv^2)],$$

$$q_{\max} = \hbar^{-1}(K + K'),$$

where  $\theta$  is the polar ejection angle of the electron,  $\Delta E$  is the transferred energy, and  $M$  is the mass of the incident ion. Since  $q_{\max}$  is usually very large in atomic collisions, one can set it equal to infinity. Integration over  $q$  in (2) is done numerically. [Equation (2) was derived in (KJ63), but a misprint has been corrected here.]

Electron energy distributions for other colliding systems can be estimated using the scaling procedure

$$(d\sigma/dE_e)(z, I, E, E_e, n) = nz^2(I_H/I)^3 (d\sigma/dE_e) \times [1, I_H, 1, E(I_H/I), E_e(I_H/I), 1], \quad (3)$$

where  $z$  and  $E$  are the charge and energy of the incident ion, respectively,  $I$  and  $I_H$  are the ionization potentials of the target and hydrogen atom,  $E_e$  is the ejected electron energy, and  $n$  is the number of electrons in the ionized atomic shell. [Equation (3) was derived in (RSB66) for  $Z=1$ .]

The method described in (BG53) was used later in calculations of energy distributions of electrons ejected in collisions of  $\text{He}^{2+}-\text{He}$ ,  $\text{H}^+-\text{Li}$ , and  $\text{H}^+-\text{Ne}$  (E54; BDO57; DP61) at energies of relative motion ranging from several tens of kiloelectron volts to several thousand kiloelectronvolts.

### B. Classical Binary-Encounter Approximation

Gryzinski (G59,65) has developed a classical approach to the problem of excitation and ionization in electronic and atomic collisions. In the binary-encounter approximation used by the author, an interaction is considered between two classical particles, the incident ion (or electron) and the atomic electron. The atomic features of the latter are taken into account by introducing a proper velocity distribution function. The

energy transferred to the atomic electron in the collision can be found from the energy and momentum conservation laws as a function of the scattering angle. Then the cross section for the appropriate inelastic process can be obtained using the relation between the impact parameter and the scattering angle for the Coulomb interaction.

The classical approach was used by Bonsen and Vriens (BV70) in calculations of energy and angular distribution of electrons ejected in ion-atom collisions. The doubly differential cross section for the electron ejection was obtained as

$$\frac{d^2\sigma}{dE_e d\Omega} = n \int_{v_2 \min}^{v_2 \max} \sigma'(v_2, E, v_1, \theta) f(v_2) dv_2, \quad (4)$$

where  $n$  is the number of electrons in the ionized atomic shell,  $v_1$  and  $v_2$  are the initial velocities of the incident ion and atomic electron,  $E$  is the transferred energy equal to the sum of the ionization potential and kinetic energy of the ejected electron, and  $\theta$  is the electron ejection angle. Neglecting the terms proportional to the ratio  $m/M$  of the electron mass to the incident ion, we can obtain the differential cross section  $\sigma'(v_2, E, v_1, \theta)$

$$\begin{aligned} \sigma'(v_2, E, v_1, \theta) &= (z^2 e^4 v_1 v_2' / 2m v_2 E^3) \\ &\times \{m v_2'^2 \sin^2 \theta - E[1 - (v_2'/v_1) \cos \theta]\} \\ &\times (v_1^2 + v_2'^2 - 2v_1 v_2' \cos \theta)^{-3/2}, \quad (5) \end{aligned}$$

where  $ze$  is the incident ion charge and

$$v_2' = [v_2^2 + (2E/m)]^{1/2}.$$

The values  $v_{2 \min}$  and  $v_{2 \max}$  can be found from energy and momentum conservation (BV70).

The distribution  $f(v_2)dv_2$  is obtained from the representation of the electron wave function in the momentum space

$$\Psi_{nlm}(\mathbf{p}) = (2\pi\hbar)^{-3/2} \int_0^\infty \Psi_{nlm}(\mathbf{r}) \exp\left(-\frac{i\mathbf{p}\mathbf{r}}{\hbar}\right) d\mathbf{r}, \quad (6)$$

and

$$f(p) dp = 4\pi p^2 dp [(2l+1)^{-1} \sum_{m=-l}^l |\Psi_{nlm}(\mathbf{p})|^2]. \quad (7)$$

The use of the hydrogen 1s wave function yields

$$f(v_2) dv_2 = (32/\pi) [v_2^2 v_0^3 / (v_2^2 + v_0^2)^4] dv_2, \quad (8)$$

where  $v_0 = (2I_H/m)^{1/2}$ .

Applications of the Born approximation and the classical approach are limited to cases in which relative velocities are higher than the orbital velocity of atomic electrons and the colliding particles are simple atomic systems.

### C. Statistical Models

In the case of collisions between complex many-electron atomic systems it is reasonable to use a statistical approach to the study of ionization phenomena.

In the statistical model advanced by Russek and Thomas (RT58) ionization is treated as an "evaporation" of electrons from the atom "heated" by a collision. The excitation energy acquired by the atomic particles after the collision is distributed statistically among the outer shell electrons. As a result, one or more electrons can gain enough energy for their removal from the atom. In this approximation the probability that the atom will become  $n$ -fold ionized is defined by the number of ways in which the excitation energy  $E_T$  can be distributed among  $N$  atomic electrons, so that  $n$  of them receive the energy needed for their removal.

The statistical model of Russek and Thomas was used earlier in interpretation of experimental data on relative probability of multiple ionization and angular distributions of multiply charged ions formed in atomic collisions. Recently this model has been adjusted to the calculations of energy distribution of the ejected electrons (RM70).

In the new version of the model, the ionization process is divided into two stages. In the initial stage the formation of a quasimolecule occurs, followed by a strong excitation of electron shells. In the final stage, the excited states of atoms decay via autoionization. The initial excitation process is considered in this model only as a source of the excitation energy  $E_T$ . De-excitation occurring in the final stage is assumed to be of statistical character.

Assuming equal *a priori* probability per unit volume of momentum space, the relative energy distribution  $dN/dE_e$  of the ejected electrons can be written as (RM70)

$$\begin{aligned} \frac{dN}{dE_e} &= \epsilon_1^{-1} \left[ \sum_{n=1}^N n \binom{N}{n} g^n S_{n-1} \left( \frac{E_k - E_e}{\epsilon_1} \right) S_1 \left( \frac{E_e}{\epsilon_1} \right) \right] / \sum_{n=1}^N \binom{N}{n} g^n S_n \left( \frac{E_k}{\epsilon_1} \right), \\ S_n(E) &= \frac{2^{l(n+1)/2} \pi^{[n/2]} E^{(3n-2)/2}}{2(3n-2)!!}, \\ (3n-2)!! &= (3n-2)(3n-4)\cdots k, \\ k &= 2 \quad \text{for even } n \\ &= 1 \quad \text{for odd } n, \end{aligned} \quad (9)$$

where  $E_k$  is the fraction of the total excitation energy  $E_T$  converted into kinetic energy of electrons,  $\epsilon_1$  is the first ionization potential, and  $\binom{N}{n}$  is the binomial coefficient determining the number of ways in which  $n$  ejected electrons can be selected from  $N$  electrons of an atomic shell. The factor  $S_n(E)$  characterizes energy dependence of the energy state density in a unit volume of phase space. The statistical weight  $g$  is proportional to the average probability of transition from the initial state to one of the states of the  $n$ -fold ionized atom. The factor  $g$  is chosen as a parameter and it is usually set equal to unity. The sign [ ] stands for the integral part of the value in the brackets.

The absolute values of differential cross sections are obtained as

$$d\sigma/dE_e = 2\pi \int [dN(E_e, E_T, N)/dE_e] \rho(E_T) d\rho(E_T), \quad (10)$$

where  $\rho$  is the impact parameter. Since Russek's model does not consider the excitation process, this model per se contains no information about the dependence of the transferred energy on the impact parameter, i.e., about the absolute values of cross sections. Therefore, the function  $\rho(E_T)$  in (10) should be obtained either from experimental data on inelastic energy loss spectrum, or from independent calculations.

Another statistical model was advanced by Firsov (F59). In this model, excitation of atoms in atomic collisions is considered as a result of mutual "deceleration" of nuclei caused by the momentum exchange between the electrons belonging to the colliding particles. In this process a certain fraction of energy of relative motion is converted into the electron excitation energy, which gives rise to ionization after or nearly after the collision.

The advantage of Firsov's theory is that it makes it possible to determine the excitation energy as a function of the impact parameter and, hence, to calculate the absolute values of the ionization cross sections. The total ionization cross section is given by the formula

$$\sigma = \sigma_0 \left[ (v/v_0)^{1/5} - 1 \right]^2, \quad \text{cm}^2 \quad (11)$$

where  $v_0 = 23.3 \times 10^6 \epsilon_i / (Z_1 + Z_2)^{5/3}$  cm/sec,  $\sigma_0 = 32.7 \times 10^{-16} / (Z_1 + Z_2)^{2/3}$  cm<sup>2</sup>,  $v$  is the relative velocity in cm/sec,  $\epsilon_i$  is the ionization energy in eV, and  $Z_1$  and  $Z_2$  are the nuclear charges of the respective colliding particles. If the excitation energy  $E_T$ , including the kinetic energy of ejected electrons, is substituted into the formula for  $v_0$  instead of the ionization energy, then the differential cross section for energy transfer ranging from  $E_T$  to  $E_T + dE_T$  can be obtained by differentiating formula (11) to obtain

$$\frac{d\sigma}{dE_T} = \frac{9.3 \times 10^6}{(z_1 + z_2)^{5/3}} \frac{\sigma_0}{v_0} \left( \frac{v}{v_0} \right)^{1/5} \left[ \left( \frac{v}{v_0} \right)^{1/5} - 1 \right], \quad \text{cm}^2/\text{eV}. \quad (12)$$

The energy distribution of ejected electrons can be

written as

$$d\sigma/dE_e = \int (d\sigma/dE_T) (dN/dE_e) dE_T, \quad (13)$$

where the function  $dN/dE_e$  can be taken, for example, from Eq. (9).

The main difficulty that the statistical models meet when used in calculations of electron energy distributions is the impossibility of making correct allowance for optical excitation. In fact, a certain fraction of the total excitation energy  $E_T$  can be transferred to the optical excitation of the electrons. It is difficult to estimate the contribution of this process concurrent to electron ejection to the continuum.

#### D. Autoionization

The theoretical methods and models discussed in the previous sections describe the processes which produce the continuous energy distribution of the ejected electrons. These processes are associated either with direct transition of the atomic electron to a continuum state (the Born approximation, the binary-encounter approximation) or with statistical distribution of the excitation energy among many electrons (statistical models). There may be also the situation in which the electron transition to the continuum occurs via an intermediate autoionization state. Such transitions are monoenergetic and they result in the appearance of discrete lines in the electron energy spectrum.

One of the possibilities for the formation of an autoionization state is caused by the simultaneous excitation of two electrons, for example,  $2s^2$  He. De-excitation of this state occurs via a radiationless transition in which one of the electrons fills the vacancy in the  $1s$  shell of the helium atom, and the other is ejected into continuum with a fixed kinetic energy ( $2s^2$  He  $\rightarrow$   $1s$  He<sup>+</sup> +  $e^-$ ).

An autoionization state can also be formed as a result of single electron excitation. For example, such a possibility in the case of noble gas atoms is caused by the existence of two ionization limits corresponding to the ion states  $^2P_{3/2}$  and  $^2P_{1/2}$ . Highly excited levels converging to the upper limit  $^2P_{1/2}$  become autoionizing ones with respect to the lower limit  $^2P_{3/2}$ . Another possibility for the formation of an autoionization state in single electron excitation is connected with the creation of a vacancy in the inner subshell (e.g.,  $1s^2 2s 2p^6 3p$  Ne) or the inner shell (e.g.,  $1s 2s^2 2p^6$  Ne) of the atom. Decay of the autoionization states of the latter type is usually called the Auger effect. Classification of the Auger transitions is made both in the notations of optical spectroscopy used above and in the notations accepted in x-ray spectroscopy, where configurations are labeled by the states of "holes", for example,  $K-L_1L_1$ .

The probability of an autoionization transition in the nonrelativistic approximation is given by the

formula

$$W = (2\pi/\hbar) \left| \int \Psi_f^*(1, 2) (e^2/r_{12}) \Psi_i(1, 2) d\mathbf{r}_1 d\mathbf{r}_2 \right|^2, \quad (14)$$

where  $\Psi_i$  and  $\Psi_f$  are the wave functions of the initial and final states, respectively of two electrons involved in the transition, the electrostatic interaction  $e^2/r_{12}$  between the electrons being considered as a perturbation. Theoretical calculations (RR37; RS55; C61; A65) show that the values of Auger transition probabilities range from  $10^{12}$  to  $10^{15}$  sec $^{-1}$ .

The energy  $E_e$  of electrons ejected in the Auger transition  $V$ - $XY$  is defined by the equation

$$E_e = E(V) - E^Z(X) - E^{Z+1}(Y), \quad (15)$$

where  $E(V)$  is the binding energy of one electron in the subshell  $V$ , in which the initial vacancy is created,  $E^Z(X)$  is the binding energy of an electron of the subshell  $X$  which fills the vacancy, and  $E^{Z+1}(Y)$  is the binding energy of an electron in the subshell  $Y$  of the atom singly ionized in the subshell  $X$ . If the subshell  $X$  is the inner one with respect to the subshell  $Y$ , one can use for  $E^{Z+1}(Y)$  the binding energy of the electron in the subshell  $Y$  of the atom following this one in the periodic system. This approximation is based on the assumption that the formation of a vacancy in an inner shell is equivalent to the increase in the nuclear charge by unity. In the case of autoionization transitions from the initial states in which one or two electrons occupy excited optical levels the energy  $E_e$  can be found from the equation (S63):

$$E_e = E_{e\infty} - [13.6Z_n^2/(n-\mu)^2], \quad (16)$$

where  $E_{e\infty}$  is the energy of the series limit counted with respect to the final ion state,  $Z_n$  is the charge of the final state configuration,  $n$  is the principal quantum number, and  $\mu$  is the quantum defect. The values of  $E_{e\infty}$  are usually well known from spectroscopic tables, and the quantum defect  $\mu$  can be determined using the following empirical rules:

(1) The quantum defect of the atomic state with an excited inner shell electron is approximately equal to that of the similar state of the atom following this one in the periodic table. For example, the configuration  $3s3p^64p$  of ArI corresponds to the configuration  $3s^23p^64p$  of KI.

(2) When passing to the heavier atom of the same group in the periodic table (e.g., from Ne to Ar), the quantum defect increases by unity.

In the case of Ar, rules (1) and (2) give values of electron energies which are uncertain by 0.1 eV and 0.3 eV, respectively (S63; OFA69a).

An autoionization transition becomes possible when certain selection rules are obeyed. If the perturbation

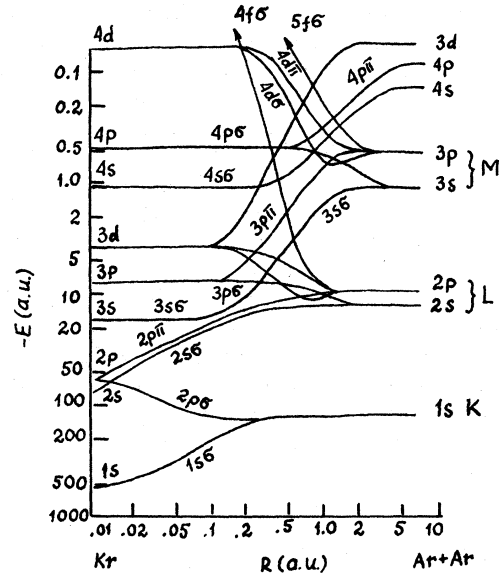


FIG. 1. Energy levels of diabatic molecular orbitals of the Ar+Ar system (FL65).

inducing the transition is the Coulomb interaction of electrons, then these rules require that the initial autoionization state and the final state of the system ion plus ejected electron must have the same parity  $\pi$  and angular momentum  $J$ . In the case of  $LS$  coupling, when the values of the angular momentum  $L$  and the spin  $S$  are good quantum numbers, two rules requiring the conservation of the values  $L$  and  $S$  are added. Thus, the selection rules for  $LS$  coupling are

$$\Delta\pi = \Delta J = \Delta L = \Delta S = 0. \quad (17)$$

The selection rules imposed on  $L$  and  $S$  are satisfied strictly only for the lightest atomic systems. In the case of noble gas atoms a breakdown of  $LS$  coupling and appearance of spectral lines associated with forbidden autoionization transitions is observed even in argon (M67; V68).

Of considerable influence on the intensity sharing of the spectral lines is the configuration interaction in the initial and final states. Due to this effect a certain initial or final state may be represented by a mixture of identical terms of different configurations. In some cases the admixture of the "foreign" states appears very large. For example, in the case of  $K$ - $LL$  transitions in argon, strong coupling of the final states  $2s^02p^6(^1S)$  and  $2s^22p^4(^1S)$  is taking place (AM68). A detailed theoretical study of the configuration interaction in the initial state has been carried out only for the autoionization states in helium (AlMo66; BuMcV65; BGKS68). In that case the configuration interaction was found to be considerable. It was especially strong for the coupling of the configurations which differed only in the orbital momenta, e.g.,  $2s3p$  and  $2p3s$ .

The features of the autoionization processes discussed

above are relevant to the transitions in an isolated atom, i.e., in a spherically symmetrical system. In recent years a few papers have been published (KP67; Sm67) in which the probability of autoionization transitions is studied when spherical symmetry is destroyed by the formation of a quasimolecule. Kishinevsky and Parilis (KP67) have considered the transition probability in the quasimolecule consisting of two electrons moving in the field of two Coulomb centers. It was shown in (KP67) that at a certain internuclear separation  $R \sim a_0$  the transition probability became about two orders of magnitude higher than that in the isolated atom. This result indicates an important role of the autoionization transitions in a quasimolecule and may be extended to the cases of more complex colliding systems. It should be noted that autoionization transitions in a quasimolecule give rise to a continuous energy distribution of the ejected electrons (Sm67).

### E. Molecular Orbital Theory

The behavior of energy levels in a quasimolecule can be responsible for the formation of the inner shell vacancies in the colliding particles. Calculations of the molecular energy levels are very difficult and can be made analytically only for the system of one electron in the field of two Coulomb centers. An important role in the calculations of many-electron molecular systems is played by the molecular orbital approximation (Hund-

Mulliken approximation) in which each electron of the system is considered as moving independently in a self-consistent field of nuclei and other electrons, and is characterized by its own quantum numbers.

One of the problems arising in calculations of the molecular (or quasimolecular) levels consists in establishing the correlation between the electron states in isolated atoms at  $R \rightarrow \infty$  and those of the united atom to which the appropriate orbitals converge at  $R \rightarrow 0$ . For two identical Coulomb centers, the correlation rules were established by Morse and Stückelberg (MS29),

$$\left. \begin{aligned} l &= 2n_2 + |m| \\ N &= n + n_2 \end{aligned} \right\} \text{for gerade states}$$

$$\left. \begin{aligned} l &= 2n_2 + |m| + 1 \\ N &= n + n_2 + 1 \end{aligned} \right\} \text{for ungerade states, (18)}$$

where  $N$  and  $l$  are the quantum numbers of the electron in the united atom,  $|m|$  is the projection of the orbital momentum along the internuclear axis, and  $n = n_1 + n_2 + |m| + 1$  is the principal quantum number of the electron in an isolated atom at  $R \rightarrow \infty$ ;  $n_1$  and  $n_2$  being the parabolic quantum numbers.

For two different Coulomb centers ( $Z_1 < Z_2$ ), the correlation rules were established by Gershtein and Krivchenkov (GK61).

(A) The electron is located in the vicinity of the nucleus  $Z_1$  at  $R \rightarrow \infty$ .

$$l = \begin{cases} n_2 + |m| + 1 + [n_2 + n(z_2 - z_1)/z_1], & \text{when } (z_2/z_1)n \text{ is not an integer} \\ 2n_2 + |m| + n[(z_2 - z_1)/z_1], & \text{when } (z_2/z_1)n \text{ is an integer} \end{cases}$$

$$N = \begin{cases} n + 1 + [n_2 + n(z_2 - z_1)/z_1], & \text{when } (z_2/z_1)n \text{ is not an integer} \\ n_2 + n(z_2/z_1), & \text{when } (z_2/z_1)n \text{ is an integer} \end{cases} \quad (19)$$

(B) The electron is located in the vicinity of the nucleus  $Z_2$  at  $R \rightarrow \infty$ .

$$l = \begin{cases} n_2 + |m|, & \text{when } n_2 < n[(z_2 - z_1)/z_2] \\ n_2 + |m| + 1 + [n_2 - n(z_2 - z_1)/z_2], & \text{when } n_2 \leq n[(z_2 - z_1)/z_2] \end{cases}$$

$$N = \begin{cases} n, & \text{when } n_2 < n[(z_2 - z_1)/z_2] \\ n + 1 + [n_2 - n(z_2 - z_1)/z_2], & \text{when } n_2 \leq n[(z_2 - z_1)/z_2] \end{cases}$$

where  $[ \ ]$  stands for the integral part of the value in the brackets.

The case of the Coulomb field is specific in that it allows the violation of the Wigner-Neumann theorem about noncrossing of orbitals of the same symmetry (Be33; GK61). In a quasimolecule formed in the collisions of many-electron atoms, the field will differ from the Coulomb field. However, if the velocity of relative motion is high enough to make the splitting of

the interacting levels negligible, one can suggest (L63) that the behavior of the levels will be the same as in the case of the Coulomb field ("adiabatic" behavior of levels). Using this assumption, Fano and Lichten (FL65) have drawn the energy level diagrams of quasimolecules formed in  $\text{Ne}^+ - \text{Ne}$  and  $\text{Ar}^+ - \text{Ar}$  collisions (the latter is shown in Fig. 1). These authors (FL65) have come to the conclusion that a "promotion" of levels corresponding to the inner shells of atoms can

occur in these cases. The "promoted" level can cross a number of unfilled orbitals corresponding to the outer shells, and transitions between molecular orbitals at crossings will lead to the creation of the inner shell vacancy after collision. In particular, the creation of a  $L_{2,3}$  vacancy in  $\text{Ar}^+-\text{Ar}$  collisions can be caused by the "promotion" of the  $4f\sigma$  orbital (see Fig. 1).

Lichten (L67) has considered the main types of transitions that give rise to excitation of atomic particles after collision. They can be divided into single-electron transitions and transitions in which two or more electrons are involved. The former are possible when proper selection rules are satisfied. If the Coulomb interaction of electrons is the perturbation which induces the transition, the selection rule  $\Delta m=0$  must be obeyed, i.e., the transitions are possible only between the orbitals of the same symmetry ( $\sigma-\sigma$ ,  $\pi-\pi$ , etc). Single-electron transitions due to rotation of the internuclear axis are possible when  $m=\pm 1$ , i.e., the transitions  $\sigma\leftrightarrow\pi$ ,  $\pi\leftrightarrow\delta$ , etc. are allowed. Transitions of two or more electrons obey the selection rules requiring conservation of the summed values of quantum numbers, so they are allowed practically for any  $\Delta m$ .

The theoretical methods and models considered in this section represent the background which underlies our ideas of ionization processes in ion-atom collisions. They will be used below in the interpretation of experimental data on electron energy spectra.

## 2. EXPERIMENTAL RESULTS AND DISCUSSION

Before beginning the review of experimental data on electron energy spectra it is reasonable to outline the experimental technique and the character of the information obtained.

### A. Experimental Technique

The main elements of an apparatus used in experiments on energy spectra of electrons ejected in ion-atom collisions are the ion source, the electron energy analyzer, and the detector of electrons. The most important part of the apparatus, its heart, is the electron energy analyzer.

Methods for energy analysis of charged particles have not changed considerably during the last decades. The well known types of analyzers such as the parallel plate condenser, the  $127^\circ$  cylindrical analyzer, and the cylindrical electrostatic mirror are still widely used. These analyzers are reliable in operation and yield a resolution  $\Delta E/E$  of 1% to 3% in normal experimental conditions. The resolution can be improved by applying a retarding potential to the whole analyzer system and varying it, the potential between the analyzer electrodes being maintained constant. However, the use of this method gives rise to additional errors due to the focusing effect at the entrance slits (V68).

Considerable difficulty arises in measurements at low

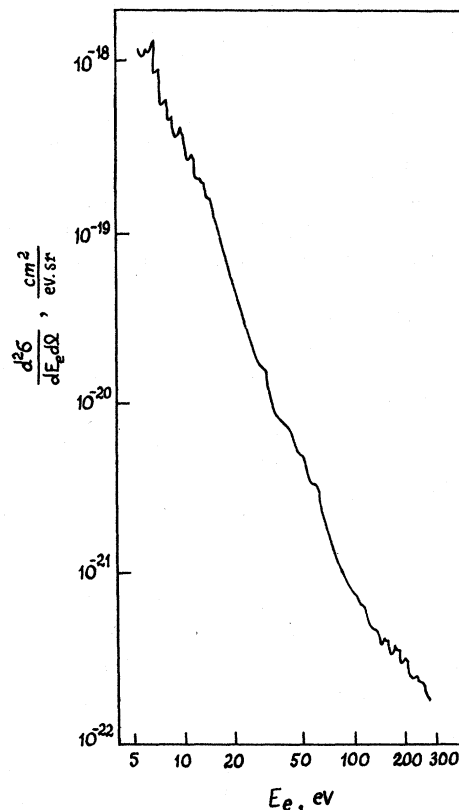


FIG. 2. Energy distribution of electrons ejected in  $\text{H}^+-\text{Ar}$  collisions at the proton energy  $E_p=20$  keV and electron ejection angle  $\theta=54.5^\circ$  (OFA69a).

and high electron energies. In the former case, these difficulties are connected with the strong scattering of slow electrons, the influence of weak electric and magnetic fields, and other unwanted effects. The use of pre-acceleration by a positive potential applied to the entrance slit increases the uncertainty in the dimensions of the electron extraction region and leads to the focusing effect mentioned above. Of great importance in experiments with slow electrons is the precise compensation for the residual magnetic field. In investigations of high-energy electrons the main difficulty comes from very small cross sections for electron ejection. In such measurements it is desirable to use an analyzer with a large effective solid angle, for example, the cylindrical electrostatic mirror (OFA69b). However, measurements of a wide range of electron ejection angles are impossible in this case. In practice, none of the available types of analyzers can meet all the requirements of high resolution, large effective solid angle, and possibility of measurements in a wide range of electron energies and ejection angles. Therefore, the choice of analyzer to be used in an experiment depends on the character of the problem under study.

The progress in the experimental study of electron

energy spectra made in recent years is largely due to the progress in the development of methods for registering charged particles. Transition from measurements of the total electron current to single-electron counting by electron multipliers with very low noise has led to increasing sensitivity of experimental technique. At present it is possible to measure differential cross sections as low as  $10^{-21}$  and  $10^{-22}$   $\text{cm}^2/\text{eV}\cdot\text{sr}$ , with relative errors of about 5%–10%. Larger errors appear in the measurements of absolute values of the differential cross sections. These errors are composed of the errors in measuring the pressure, geometrical parameters of the analyzer, and the detector efficiency. In most experiments discussed below, the errors in the measurements of absolute cross sections were  $\pm(30\%-50\%)$ .

The shape of the energy distribution of electrons ejected in atomic collisions is usually rather complicated. As an example, such a distribution is shown in Fig. 2 measured by (OFA69a) for the colliding pair  $\text{H}^+-\text{Ar}$ . Two parts can be discerned in this distribution, a continuous background falling off smoothly with increasing electron energy and a discrete structure associated with autoionization transitions in the target atom. Correspondingly, two kinds of problems being solved in experiments can be defined. They are:

(1) Measurements of the absolute values of cross sections for electron ejection, their dependence on the incident ion energy, and the electron energy and ejection angle.

(2) The study of structure in electron energy spectra, determination of autoionization state energies, and determination of probabilities of autoionization transitions. Certainly, this method of autoionization state spectroscopy can hardly compete in accuracy with the photoabsorption method. Nevertheless, it has evident advantages due to the possibility of measurements in a very wide range of electron energies and as a means of studying practically all autoionization states of the colliding particles rather than only those allowed by the selection rules for dipole transitions. Besides, the study of structure in electron energy spectra provides information on the modes of the autoionization state decay which can not be obtained by the photoabsorption method.

In the following sections some experimental results on energy spectra of electrons ejected in ion-atom collisions will be discussed and their possible theoretical interpretation will be given. In cases in which some discrepancy between theory and experiment is noted, it will mean that this discrepancy is considerably larger than the experimental errors.

### B. Collisions Between Two Light Atomic Particles

It seems reasonable to begin a review of experimental data with a discussion of such processes in which both

colliding partners are relatively simple atomic systems, e.g.,  $\text{H}^+-\text{H}_2$ . In this case, the shape of the electron energy distribution is not complicated by the structure associated with autoionization transitions. If the incident proton velocity is higher than the orbital velocity of atomic electrons then a direct comparison is possible between experimental data and the Born or binary-encounter calculations for the hydrogen atom. (At high proton velocities one can use the relation  $\sigma(\text{H}_2) = 2\sigma(\text{H})$ ). (Compare, for example, S69).

Almost all results available on energy spectra of electrons ejected in  $\text{H}^+-\text{H}_2$  collisions have been obtained by Rudd and coworkers (RSB66) in the proton energy range 100–300 keV in which the Born approximation is valid. In (RSB66; RG69) the experimental data on the doubly differential cross sections ( $d^2\sigma/dE_e d\Omega$ ) and the cross sections integrated over the electron energy ( $\int (d^2\sigma/dE_e d\Omega) dE_e$ ) and the ejection angle ( $\int (d^2\sigma/dE_e d\Omega) \sin\theta d\theta$ ) were compared to those obtained in the Born and binary encounter calculations. It was found that a reasonable agreement between the experimental data and the Born calculations was observed only for the values  $\int (d^2\sigma/dE_e d\Omega) \sin\theta d\theta$ . The classical binary-encounter calculations with the velocity distribution of atomic electrons obtained from the wave function in momentum space [Eq. (6.7)] also agree with the experimental results (Fig. 3). The agreement between theory and experiment becomes much

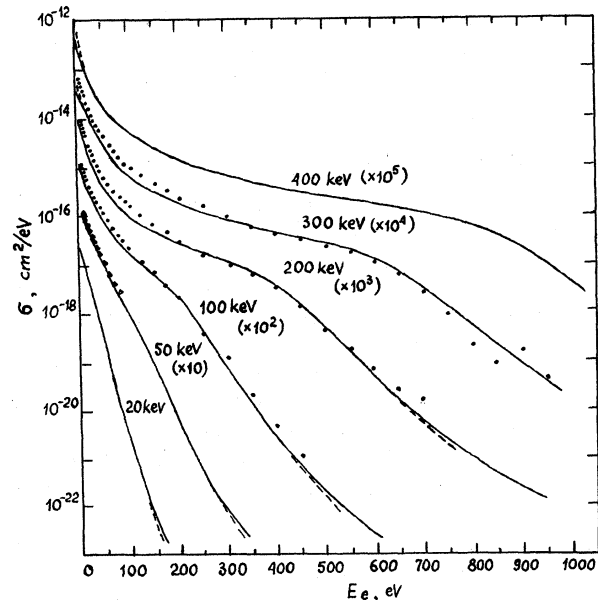


Fig. 3. Differential cross sections for electron ejection from proton impacts on  $\text{H}_2$ . Experimental data (RSB66) (points), and (KJ63) (triangles) are compared with Born approximation (broken line) and classical binary-encounter calculations (solid line). The values of the proton energy are given in the figure (RG69, p. 795).

poorer when the cross sections ( $d^2\sigma/dE_e d\Omega$ ) and  $\int (d^2\sigma/dE_e d\Omega) dE_e$  are analyzed. In the latter case the discrepancy between experimental results and calculations sometimes reaches values of about an order of magnitude.

One of the reasons for this discrepancy is connected with the fact that the usual Born approximation neglects long-range interaction between the ejected electron and the scattered proton. The electron is supposed to move in the field of the ionized target atom. This is valid only for electrons ejected with velocities much smaller than those of the incident

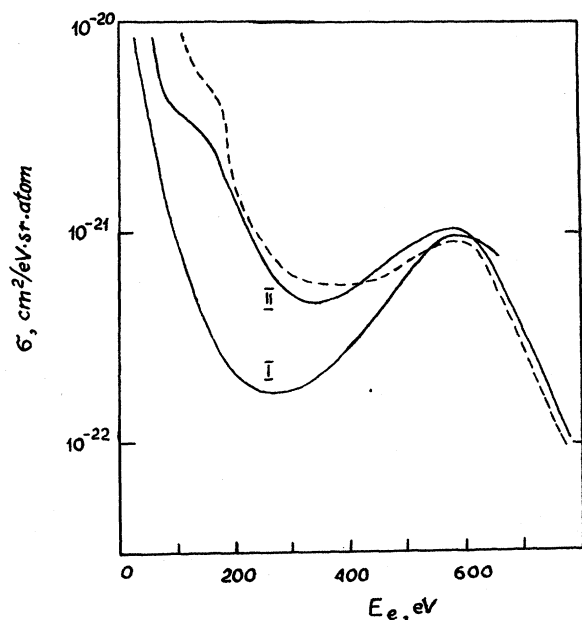


FIG. 4. Energy distribution of electrons ejected in  $H^+-H_2$  collisions at the proton energy  $E_p=300$  keV, and electron ejection angle  $\theta=10^\circ$ . Broken line, experiment (RSB66); I, Born approximation with  $Z=1$ ; II, Born approximation with  $Z_{eff}$  defined by the formula (20) (Sa69).

proton. In the general case the "effective" charge in whose field the ejected electron moves is dependent on the electron velocity.

Salin (Sa69) has calculated the energy distribution of electrons ejected in  $H^+-H_2$  collisions at the proton energy 300 keV, using the Born approximation with the effective charge  $z_{eff}$  obtained as

$$z_{eff} = 1 + (\kappa/|\kappa - \mathbf{v}|), \quad (20)$$

where  $\kappa$  and  $\mathbf{v}$  are the velocities of the ejected electron and the incident proton, respectively. In this approximation the matrix element  $R(\mathbf{q}, \kappa)$  (see Eq. 1) can be related in a simple way to the matrix element  $R_0(\mathbf{q}, \kappa)$

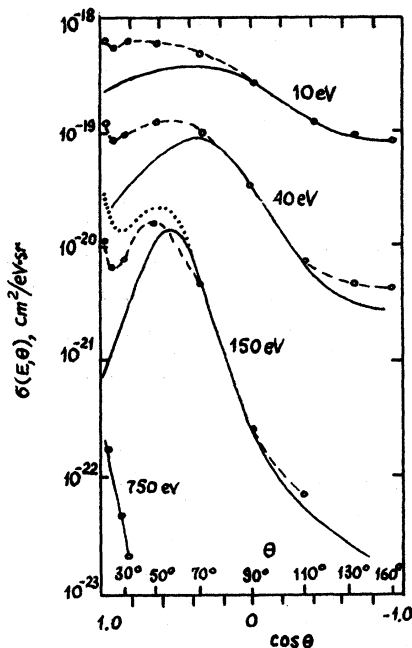


FIG. 5. Angular distribution of electrons ejected in  $H^+-H_2$  collisions at the proton energy  $E_p=300$  keV. Broken line, experiment (RSB66); solid line, Born approximation; dotted line, calculations (Ma70).

calculated in the first Born approximation

$$|R(\mathbf{q}, \kappa)|^2 = \{2\pi\gamma/[1 - \exp(-2\pi\gamma)]\} |R_0(\mathbf{q}, \kappa)|^2, \quad (21)$$

where  $\gamma = [1/(|\mathbf{v} - \kappa|)] - (1/v)$ .

Comparison between the calculations (Sa69) and the experimental results obtained by Rudd and co-workers (RSB66) is given in Fig. 4. This comparison shows that the approximation used by Salin leads to much better agreement with experiment than the standard Born approximation (BG53).

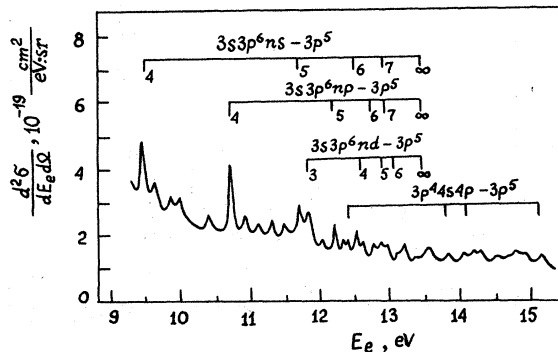


FIG. 6. Energy spectrum of electrons ejected in  $H^+-Ar$  collisions at the proton energy  $E_p=20$  keV and electron ejection angle  $\theta=54.5^\circ$  (OFA 69a). Autoionization transitions  $3s3p^6 nl-3p^5$  and  $3p^4 4s4p-3p^5$ .

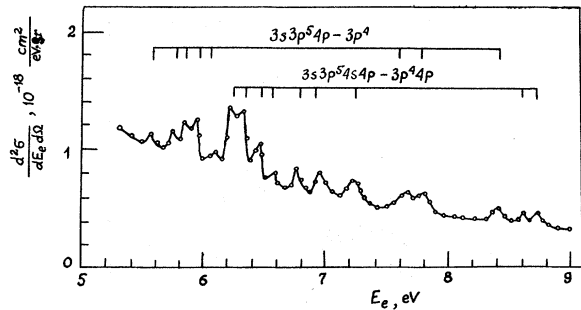


FIG. 7. Energy spectrum of electrons ejected in  $H^+-Ar$  collisions at the proton energy  $E_p=20$  keV and electron ejection angle  $\theta=54.5^\circ$  (OFA69a). Autoionization transitions  $3s3p^5 4p-3p^4$  and  $3s3p^5 4s 4p-3p^4 4p$ .

Very large quantitative and qualitative discrepancies between Born calculations and experimental results occur when the angular distributions of ejected electrons are analyzed. Comparison of the data for  $H^+-H_2$  at the proton energy 300 keV is given in Fig. 5. In contrast to the Born calculations, experimental data show a forward peaking of the electron angular distribution at some energies of the ejected electrons. This peaking is most pronounced when the velocity of the outgoing electron is close to that of the incident proton in direction and magnitude (CR70).

Macek (Ma70) has shown that such a peculiarity in the angular distribution can be caused by interaction between the ejected electron and the receding proton after collision. In a sense, the proton captures the electron into its own continuum state, which leads to a forward peaking in the angular distribution.

In (Ma70) the approximate solution of the Faddeev equations (Fa60) for the three-body problem was used

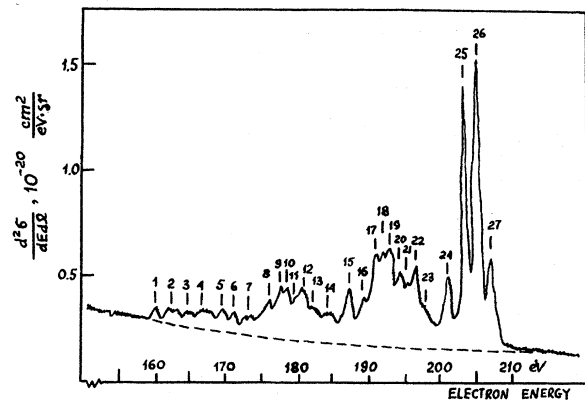


FIG. 8. Energy spectrum of electrons at  $\theta=130^\circ$  from 300 keV  $H^+-Ar$  collisions (VR70). The peaks 9, 11, 15-17, 19, 24-27 are associated with the "diagram" Auger transitions,  $L_{2,3}-MM$ . Other peaks are associated with the "satellite" transitions  $L_{2,3}M-MMM$ .

to give the final state wave function  $\Psi_f^{(-)}$  as

$$\Psi_f^{(-)} = \psi_{kep}^{(-)}(\mathbf{r}_{ep})\chi(\mathbf{R}, \mathbf{r}_{en}) + \psi_{ken}(\mathbf{r}_{en})\chi(\mathbf{R}, \mathbf{r}_{ep}) - \chi(\mathbf{R}, \mathbf{r}_{en}, \mathbf{r}_{ep}), \quad (22)$$

where  $\psi_{kep}(\mathbf{r}_{ep})$  is the Coulomb plane wave centered at the moving proton,  $\psi_{ken}(\mathbf{r}_{en})$  is the Coulomb plane wave centered at the target nucleus, and  $\chi(\mathbf{R}, \mathbf{r})$  are the products of plane waves describing the motion of the proton. The first term in [Eq. (22)] characterizes an electron moving along with the proton. If this motion is taken into account much better qualitative agreement with the experimental data is obtained (dotted curve in Fig. 5).

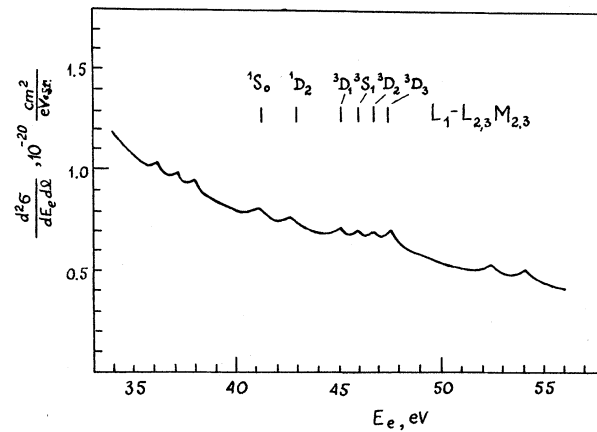


FIG. 9. Coster-Kronig transitions in  $H^+-Ar$  collisions at the proton energy  $E_p=20$  keV and electron ejection angle  $\theta=54.5^\circ$  (OFA69a). Final states of the system  $L_{2,3}M_{2,3}$  are marked in the figure. The peaks in energy range 35-38 eV are associated with the "satellite" transitions; the peaks in energy range 52-55 eV are associated with the transitions from the initial states  $2s2p^6 3s^2 3p^6 nl$ .

### C. Collisions Between Protons and Heavy Atoms

The investigations of energy spectra of electrons ejected in collisions between protons and heavy atoms are largely aimed at studying the spectroscopy of autoionization transitions. In recent years a detailed study has been carried out of the structure in the energy spectra of electrons ejected in  $H^+-Ne$  (ER68) and  $H^+-Ar$  (OFA69a) collisions. An analysis of this data leads to the following conclusions about the types of autoionization states excited by proton impact:

- (1) In excitation of the outer shell the most probable effect is the formation of autoionization states in which one of the inner subshell electrons is transferred to an excited optical level (e.g. the states  $2s2p^6 nl$  Ne and  $3s3p^6 nl$  Ar) (Fig. 6). The peaks associated with excitation of the states  $2s2p^6 ns$  and  $3s3p^6 ns$  forbidden by the selection rules for dipole transitions are rather intense. Contributions from the states  $2p^n nl n' l'$  and  $3p^n nl n' l'$  are

not so large. These states are formed as a result of two-electron excitation, although they have nearly the same excitation energy as the former ones. It has been found in (OFA69a) that the autoionization states  $3s3p^5nl$  and  $3s3p^5nl'n'l'$  could be formed in  $H^+$ -Ar collisions. The latter states have also been observed in photoabsorption experiments (MEC69). The most probable modes of their de-excitation are the transitions  $3s3p^5nl'n'l'-3s^23p^4nl(n'l')$  (Fig. 7) in which the ion is left optically excited.

(2) In excitation of the inner shells the following types of Auger transitions are possible.

(A) The "normal" or "diagram" Auger transitions (e.g.,  $K-LL$ ,  $L_{2,3}-MM$ ). The spectral lines associated with these transitions are, as a rule, the most intense (Fig. 8). A particular case of Auger transitions is represented by the Coster-Kronig transitions in which one of the inner shell electrons fills a vacancy in a deeper subshell of the same shell, and the other electron of the outer shell is ejected into continuum. These transitions are characterized by considerably lower energy than the conventional Auger transitions. The Coster-Kronig transitions  $L_1-L_{2,3}M$  have been observed in the argon atom (Fig. 9).

(B) The "satellite" transitions from the initial autoionization states of an atom ionized or excited in the outer shell (e.g.,  $2p^53s^23p^5$  Ar or  $2p^53s^23p^54s$  Ar).

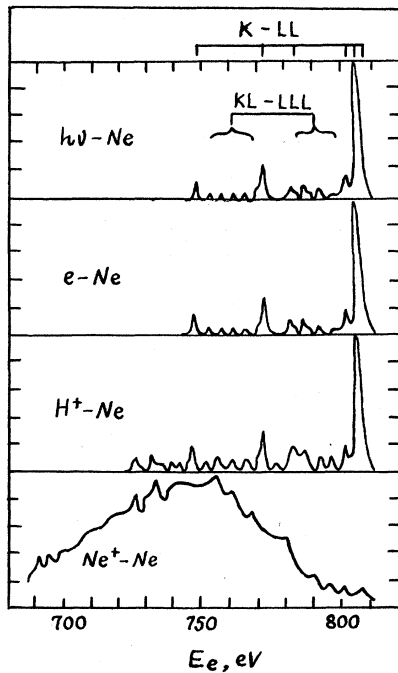


FIG. 10. Comparison between electron energy spectra associated with Auger transitions to  $K$  vacancy in neon bombarded by different projectiles:  $h\nu$ -Ne ( $E_{h\nu}=1.5$  keV) (KSLCM-70),  $e$ -Ne ( $E_e=3.2$  keV) (KSLCM70),  $H^+$ -Ne ( $E_{H^+}=300$  keV) (ER68), and  $Ne^{+}$ -Ne ( $E_{Ne^{+}}=200$  keV) (Ed67).

TABLE I. Probabilities of autoionization transitions in Ar.

| Shell                       | Transition                     | Probability,<br>( $10^{14}$ sec $^{-1}$ ) | Reference |
|-----------------------------|--------------------------------|---|-----------|
| $M$                         | $3s3p^64p(^1P)-3p^6(^2P)$      | 1.22                                      | MEC69     |
|                             | $3s3p^65p(^1P)-3p^6(^2P)$      | 0.43                                      | MEC69     |
|                             | $3s3p^66p(^1P)-3p^6(^2P)$      | 0.19                                      | MEC69     |
|                             | $3p^4(^3P)4s(^2P)4p-3p^6(^2P)$ | 0.30                                      | MEC69     |
|                             | $3p^4(^3P)3d(^2P)4p-3p^6(^2P)$ | 0.09                                      | MEC69     |
| $L_{2,3}$                   | $L_{2,3}-M_1M_1(^1S)$          | 0.13 <sup>a</sup>                         | MS68      |
|                             | $L_{2,3}-M_1M_{2,3}(^1P)$      | 0.15 <sup>a</sup>                         | MS68      |
|                             | $L_{2,3}-M_1M_{2,3}(^3P)$      | 0.23 <sup>a</sup>                         | MS68      |
|                             | $L_{2,3}-M_{2,3}M_{2,3}(^1S)$  | 0.23 <sup>a</sup>                         | MS68      |
|                             | $L_{2,3}-M_{2,3}M_{2,3}(^1D)$  | 0.88 <sup>a</sup>                         | MS68      |
|                             | $L_{2,3}-M_{2,3}M_{2,3}(^3P)$  | 0.78 <sup>a</sup>                         | MS68      |
| $L_1$                       | $L_1-M_1M_1(^1S)$              | 0.35                                      | M67       |
|                             | $L_1-M_1M_{2,3}(^1P)$          | 0.465                                     | M67       |
|                             | $L_1-M_1M_{2,3}(^3P)$          | 0.58                                      | M67       |
|                             | $L_1-M_{2,3}M_{2,3}$           | 0.05                                      | M67       |
|                             | $L_1-L_{2,3}M_1(^1P)$          | 3.13                                      | M67       |
|                             | $L_1-L_{2,3}M_1(^3P)$          | 2.37                                      | M67       |
|                             | $L_1-L_{2,3}M_{2,3}(^1S)$      | 4.10                                      | M67       |
|                             | $L_1-L_{2,3}M_{2,3}(^3S)$      | 1.70                                      | M67       |
|                             | $L_1-L_{2,3}M_{2,3}(^1P)$      | 0.335                                     | M67       |
|                             | $L_1-L_{2,3}M_{2,3}(^3P_0)$    | 0.65                                      | M67       |
|                             | $L_1-L_{2,3}M_{2,3}(^3P_1)$    | 0.385                                     | M67       |
|                             | $L_1-L_{2,3}M_{2,3}(^3P_2)$    | 0.60                                      | M67       |
|                             | $L_1-L_{2,3}M_{2,3}(^1D_2)$    | 2.85                                      | M67       |
|                             | $L_1-L_{2,3}M_{2,3}(^3D_1)$    | 1.85                                      | M67       |
|                             | $L_1-L_{2,3}M_{2,3}(^3D_2)$    | 3.25                                      | M67       |
| $L_1-L_{2,3}M_{2,3}(^3D_3)$ | 5.00                           | M67                                       |           |

<sup>a</sup> The data are averaged between the subshells  $L_2$  and  $L_3$ .

(The term "satellite" in this paper indicates all transitions of the types  $B$ ,  $C$ , and  $D$ .) The spectral lines associated with the "satellite" Auger transitions of the former type are shifted to lower energies with respect to the corresponding "diagram" lines (Fig. 8).

(C) Transitions from initial states of type  $2p^53s^22p^64p$  Ar in which the inner shell electron is transferred to an excited state rather than to the continuum. In de-excitation of such states, an optical electron can either participate directly in the transition ( $2p^53s^23p^64p-2p^63s^23p^5$ ) or act as a "spectator" ( $2p^53s^23p^64p-2p^63s^23p^44p$ ). The spectral lines associated with these transitions are shifted to higher energies with respect to the "diagram" lines.

(D) Double Auger transitions of type  $2p^53s^23p^6-2p^63s^23p^34p$  in which the energy released in the transition is distributed between two electrons, one of them being ejected into the continuum and the other being transferred to an excited optical level. The energies of these transitions are generally lower than those of "diagram" ones, and their probabilities are small. Such transitions become possible because of many-body effects in heavy atoms.

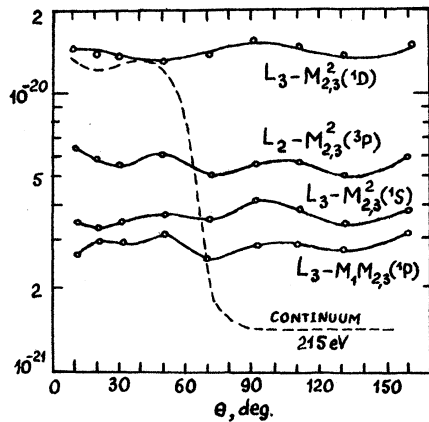


FIG. 11. Angular distribution of electrons from 300 keV  $H^+$ -Ar collisions for Auger and continuum electrons (VR70). The units of the ordinate are  $cm^2/sr$  for the Auger electrons and  $cm^2/eV \cdot sr$  for the continuum electrons.

Figure 10 shows the structure associated with  $K$ - $LL$  transitions in neon bombarded by different projectiles:  $h\nu$ -Ne,  $e$ -Ne,  $H^+$ -Ne, and  $Ne^+$ -Ne. The spectra obtained in photoionization and electron impact are practically identical, and the relative intensities of the spectral lines coincide within the experimental accuracy. In the case of  $H^+$ -Ne, the relative intensities of the "diagram" lines remain almost the same as in the previous cases but the relative yield of the "satellite" lines increases considerably. This appears to indicate the existence of a certain additional mechanism for the simultaneous formulation of vacancies in the inner and outer shells in ion-atom collisions. The spectrum for  $Ne^+$ -Ne has no resemblance to that for photoionization and electron and proton impact. This difference is associated with some specific peculiarities appropriate to collisions between two heavy atomic particles which will be discussed in the following section.

A very important subject of the study of electron energy spectra is the estimation of autoionization probabilities and life times. The estimates are usually made using experimental data on the spectral line widths and branching ratios. Only one paper on proton impact (VR70) has so far been published in which such estimates have been made for life times of autoionization states in argon. The probabilities of  $L_{2,3}$ - $MM$  transitions estimated in this work are in good agreement with those obtained in the experiments (MS68) on electron impact. The available data on the probabilities of autoionization transitions in Ar are given in Table I. It should be noted that the probabilities of autoionization transitions occurring in  $M$ - and  $L$ -shell excitation are of the same order of magnitude.

The angular distribution of electrons ejected in  $H^+$ -Ar collisions has been studied in (VR70). The continuum electrons and those ejected in  $L_{2,3}$ - $MM$  Auger transitions have been investigated individually.

The results obtained are given in Fig. 11. The angular distribution of continuum electrons ( $E_e=215$  eV) decreases rapidly with increasing ejection angle. In contrast, the angular distribution of Auger electrons proved to be nearly isotropic.

#### D. Collisions Between Two Heavy Atomic Particles

##### 1. Doppler Shift of Spectral Lines

It is essential in collisions of two many-electron atomic systems that electrons can be ejected not only from the target atom but also from the fast incident particle. If the electron is ejected from the moving particle, then its velocity vector in the laboratory system co-ordinate will be represented by a vector sum of its velocity in the emitter's frame and the velocity of the moving particle. As a result, spectral lines associated with autoionization transitions in the moving particle will be shifted from those in the stationary target particle. In the case of small scattering angles of the incident particles, the value  $\Delta E_D$  of the "Doppler" shift is defined by

$$\Delta E_D \cong mv_e v_i \cos \alpha + (mv_i^2/2) \cos 2\alpha, \quad (23)$$

where  $m$  is the electron mass,  $\alpha$  is the observation angle,  $v_e$  is the electron velocity in the emitter's frame, and  $v_i$  is the incident particle velocity.

"Doppler-shifted" spectral lines were observed in experiments (RJV66; OFA70). The presence of these lines superimposed on the "basic" lines emitted from the target atom in many cases hampers considerably the interpretation of energy spectra observed in experiments. Additional difficulties are introduced by the dependence of shape of the electron energy distribution on the incident particle velocity.

In Fig. 12 are shown the energy spectra of electrons ejected in collisions of  $Ne^+$ -Ar,  $Ar^+$ -Ne, and  $Ar^+$ -Ar (OFA70) in the electron energy range  $E_e=5-9$  eV measured at the same velocity of relative motion

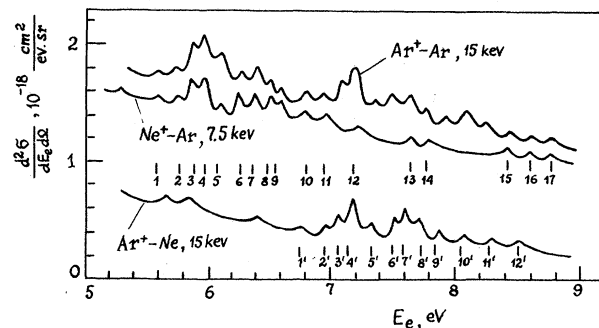


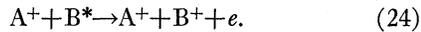
FIG. 12. Electron energy spectra for  $Ar^+$ -Ar,  $Ne^+$ -Ar, and  $Ar^+$ -Ne at the relative velocity  $v=2.7 \times 10^7$  cm/sec (OFA70) and electron ejection angle  $\theta=54.5^\circ$ . Positions of "basic" (1, 2, 3 ...) and Doppler-shifted peaks (1', 2', 3' ...) are marked in the figure.

$v = 2.7 \times 10^7$  cm/sec. "Doppler" argon lines observed in the case of  $\text{Ar}^+ - \text{Ne}$  are shifted from the "basic" ones observed in  $\text{Ne}^+ - \text{Ar}$  collisions by a value  $\Delta E_D \sim 1$  eV. In the case of  $\text{Ar}^+ - \text{Ar}$ , both basic and Doppler-shifted argon lines are observed in the spectrum; this complicates the spectrum pattern.

## 2. "Stark" Broadening of Spectral Lines

In 1961 Berry (B61), studying energy spectra of electrons ejected in collisions between ions and atoms of noble gases, found energies of some experimental peaks to fit a linear dependence on the inverse incident ion velocity. The linewidth proved to be dependent also on  $1/v$ . This effect was especially prominent in the case of  $\text{He}^+ - \text{He}$  which was carefully investigated by Barker and Berry (BB66) some years later. The authors give the following interpretation of the phenomenon observed.

Let us consider the decay of an autoionization state  $B^*$  in the Coulomb field of the receding ion  $A^+$ :



Due to Coulomb repulsion of ions in the final state of the system, the boundary of continuum and, hence, the energy of ejected electrons will depend on the internuclear separation at which the autoionization state decays. For internuclear distances much greater than the atomic dimensions one can assume

$$\begin{aligned} w(R) &= w_\infty = \text{const}, \\ E_e &= E_{e\infty} - (e^2/R), \\ dt &= (1/v) dR, \end{aligned} \quad (25)$$

where  $w(R)$  is the transition probability at a certain internuclear distance  $R$ ,  $w_\infty$  is the value of this probability in an isolated atom ( $R \rightarrow \infty$ ),  $E_e$  is the ejected electron energy,  $E_{e\infty}$  is the transition energy in an isolated atom, and  $v$  is the incident ion velocity. Starting from the decay equation

$$N = N_0 \left\{ 1 - \exp \left[ - \int^t w(R) dt \right] \right\}$$

and taking into account the relations (25), one can readily obtain the energy distribution of the electrons

$$\begin{aligned} f(E_e) &= N_0^{-1} (dN/dE_e) \\ &= [w_\infty e^2/v (E_{e\infty} - E_e)^2] \exp [-w_\infty e^2/v (E_{e\infty} - E_e)]. \end{aligned} \quad (26)$$

The distribution (26) has a maximum at the energy

$$E_{em} = E_{e\infty} - (w_\infty e^2/2v), \quad (27)$$

and the linewidth at half-maximum is

$$\gamma = 1.07 (w_\infty e^2/v). \quad (28)$$

The equations (27) and (28) explain the dependence

of the line energy and width on the incident ion velocity observed in (B61; BB66). The formula (27) is of practical importance, since the use of it allows the determination of the transition probability  $w_\infty$  or the lifetime  $\tau_\infty = (1/w_\infty)$  of an autoionization state in an isolated atom by studying the energy displacement of maxima with varied ion velocity. However, such estimate made in (BB66) for the autoionization state  $2s2p$  He has given a value  $\tau_\infty = 2.4 \times 10^{-15}$  sec which is about an order of magnitude smaller than that obtained from photoabsorption experiments (MC65) ( $1.7 \times 10^{-14}$  sec) and theoretical calculations (BMVS63) ( $1.5 \times 10^{-14}$  sec). This discrepancy has not been understood for a long time. It was not until recently that Gordeev and Ogurtsov (GO71) showed that the large width of the maximum observed in (BB66) can be due to the Doppler broadening of spectral lines which is of considerably greater influence on the shape of electron energy spectra than the Stark broadening discussed above.

## 3. Doppler Broadening of Spectral Lines

The target gas atom participating in the collision is often considered as "stationary", or only its thermal motion is taken into account. In the case of atomic collisions such an approximation is not always valid. The gas atom can gain some velocity after collision which is vectorially summed to that of the ejected electron in the emitter's frame. In atomic collisions accompanied by excitation of autoionization states, the recoil atom velocity  $v_a$  is usually much smaller than the ejected electron velocity  $v_e$ . In this case the electron energy  $E_e$  in the laboratory system coordinates can be written as

$$E_e = E_{e0} + mv_a v_e [\cos \theta_a \cos \alpha + \sin \theta_a \sin \alpha \cos (\varphi_e - \varphi_a)], \quad (29)$$

where  $E_{e0}$  is the electron energy in the emitter's frame,  $m$  is the electron mass,  $\theta_a$  is the recoil angle of the atom,  $\alpha$  is the observation angle, and  $\varphi_e$  and  $\varphi_a$  are the azimuth angles.<sup>1</sup> The first term in brackets characterizes the spectral line shift from the transition energy  $E_{e0}$  in the stationary atom. The second term in brackets describes the line broadening relative to the position of the line center  $E_{e0} + mv_a v_e \cos \theta_a \cos \alpha$ .

The latter effect (Doppler broadening of spectral lines) results in the fact that a monoenergetic line of the energy  $E_{e0}$  in the emitter's frame will be represented by a certain energy distribution of the width  $\Delta E \sim 2mv_a v_e \sin \theta_a \sin \alpha$  in the laboratory coordinate system.

In the case in which the angular distribution of ejected electrons does not differ strongly from an

<sup>1</sup> Of course, formula (29) and all the conclusions following below are applicable to the ejection of electrons from the fast incident particles, i.e., to the Doppler-shifted lines.

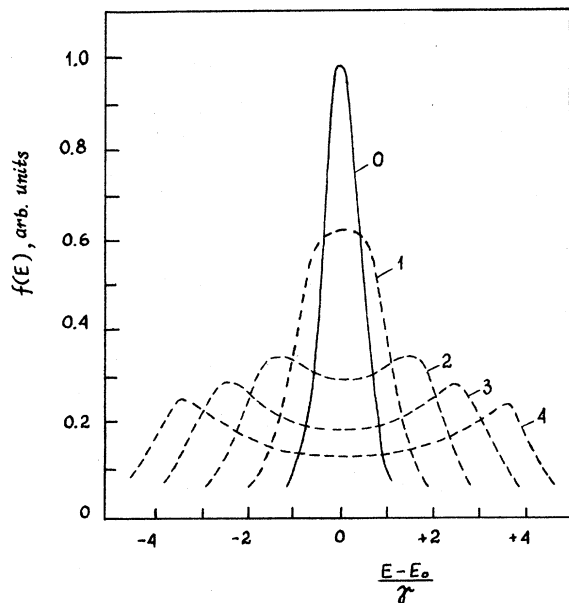


FIG. 13. Deformation of the Gaussian profile due to the Doppler effect (GO71). Figures near the profiles are the values of ratio  $B/\gamma$  (see text).

isotropic one, the energy distribution in the laboratory coordinate system corresponding to the monoenergetic line in the emitter's frame can be found as (GO71)

$$f(E_e) = N_0^{-1} (dN/dE_e) = [B^2 - (E_e - E_{e0} - A)^2]^{-1/2}, \tag{30}$$

where  $A = mv_a v_e \cos \theta_a \cos \alpha$ , and  $B = mv_a v_e \sin \theta_a \sin \alpha$ .

Figure 13 shows the deformation of the Gaussian profile of the width  $\gamma$  due to the Doppler effect calculated for different ratios  $B/\gamma$ . At large values of the Doppler width,  $B$ , the shape of the resulting profile, has no resemblance to that of the original line.

In practice, the electrons of the energy  $E_{e0}$  can be ejected from atomic particles moving with different velocities  $v_a$  and ejected at different angles  $\theta_a$ . Therefore, the distribution of the recoil particles in velocity and scattering angle should be taken into account in calculations of the line profiles. This distribution can be obtained from experimental data on inelastic energy loss spectra.

A detailed analysis (GO71) of the kinematics of inelastic collisions accompanied by considerable scattering of the atomic particles shows that in this case (e.g., see the spectrum for  $\text{Ne}^+ - \text{Ne}$  in Fig. 10) the shape of the energy spectrum reflects mainly the kinematical features of the collision rather than the real scheme of autoionization transitions.

If the original profile is a "Stark" profile [Eq. (26)], then the resulting energy distribution has an asymmetric shape with a peaked low energy edge (GO71).

Since the displacement of edges of the Doppler distribution [Eq. (30)]  $\Delta E \sim v_a \sim v \theta \sim 1/v$  ( $v$  and  $\theta$  are the velocity and scattering angle of the incident ion), the Doppler broadening leads to the same dependence of the line energy and width on the incident ion velocity as the "Stark" displacement [Eqs. (27), and (28)]. Using the experimental data (BBA69) on the inelastic energy loss spectrum in  $\text{He}^+ - \text{He}$  collisions, one can show that the Doppler broadening at ion energies of several keV is about 1 eV, i.e., the value comparable to the linewidth observed in (BB66). The shape of this line, its width, and position of the maximum are well reproduced by a superposition of broad Doppler profiles corresponding to three neighboring narrow original lines (Fig. 14). It seems evident that the displacement and broadening of spectral lines observed in (BB66) are caused mainly by the collision kinematics. The influence of the original "Stark" profile is seen only in the fact that the spectral line shifts to lower energies with increasing ion velocity.

The effects discussed above in many cases hamper the interpretation of energy spectra of electrons ejected in collisions of heavy atomic particles. If excitation of autoionization states is accompanied by strong scattering of colliding particles, then the identification of spectral lines is impossible unless the collision kinematics is taken into account. In this case the attention of investigators should be focused on studying the

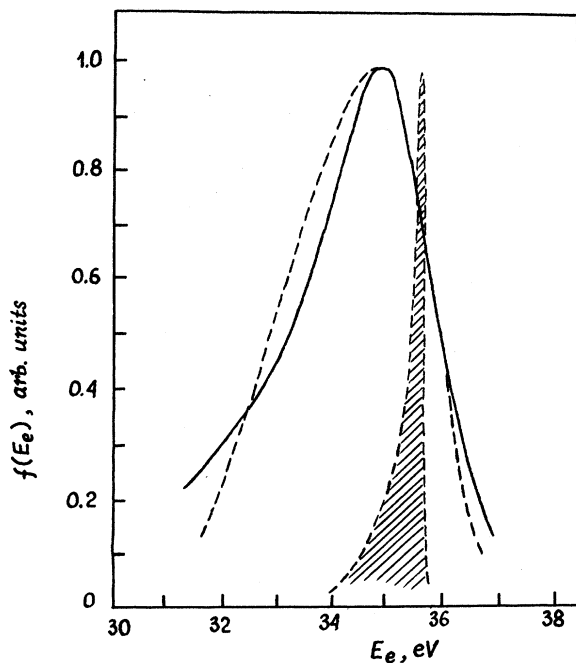


FIG. 14. Energy distribution of electrons ejected in  $\text{He}^+ - \text{He}$  collisions at the ion energy 1600 eV and electron ejection angle  $90^\circ$ . Solid line, experiment (BB66); broken line, calculations (GO71); shaded contour, one of the original lines.

integral characteristics of energy spectrum, such as cross sections corresponding to the continuous part of the spectrum and those of the inner shell excitation. The latter can be obtained by integrating the appropriate line groups over electron energy and ejection angle.

The first step in this direction was made in (CKR70; O71) where the cross sections were studied for  $L$ -shell excitation in  $\text{Ar}^+-\text{Ar}$  collisions and  $K$ -shell excitation in  $\text{Ne}^+-\text{Ne}$  collisions. The results obtained are given in Fig. 15.

As follows from the molecular orbital theory (see Fig. 1), the mechanisms for excitation of the  $L_{2,3}$  subshell of argon, on the one hand, and the  $L_1$  subshell of argon and  $K$  shell of neon, on the other hand, are different. The formation of a vacancy in the  $L_{2,3}$  subshell of argon in  $\text{Ar}^+-\text{Ar}$  collisions is caused by the "promotion" of  $4f\sigma$  orbital and its crossing with a

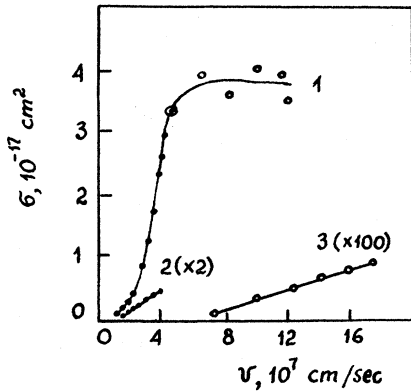


FIG. 15. Cross sections for the inner shell excitation. 1.  $L_{2,3}\text{Ar}$ ,  $\text{Ar}^+-\text{Ar}$ : points, (O71); circles, (CKR70). 2.  $L_1\text{Ar}$ ,  $\text{Ar}^+-\text{Ar}$  (O71). 3.  $K\text{Ne}$ ,  $\text{Ne}^+-\text{Ne}$  (CKR70).

number of unfilled orbitals corresponding to excited states of atoms ( $4s\sigma$ ,  $4p\pi$ ,  $3d\delta$ , etc.). It is likely that the main contribution to the cross section is given by  $\sigma-\sigma$  transitions. The dependence of the  $L_{2,3}$  subshell excitation cross section on the velocity of relative motion is represented by a smooth curve with a broad maximum (Curve 1 in Fig. 15). The cross sections are fairly large and reach values of about  $4 \times 10^{-17} \text{ cm}^2$  in the maximum region.

The formation of vacancies in the  $L_1$  subshell of argon in  $\text{Ar}^+-\text{Ar}$  collisions and in the  $K$  shell of neon in  $\text{Ne}^+-\text{Ne}$  collisions is caused by the transitions  $3p\sigma-3p\pi$  and  $2p\sigma-2p\pi$ , respectively due to rotation of the internuclear axis. This case is different from the former one not only in the kind of perturbation inducing the transition but also in the fact that the orbitals  $3p\pi$  and  $2p\pi$  correspond to filled outer shells of the atoms  $\text{Ar}$  and  $\text{Ne}$ . Therefore, the above transitions become possible only in the case in which a prior vacancy exists in the outer shell of the atom, i.e., the atom is at least singly ionized before collision. If the projectile is a

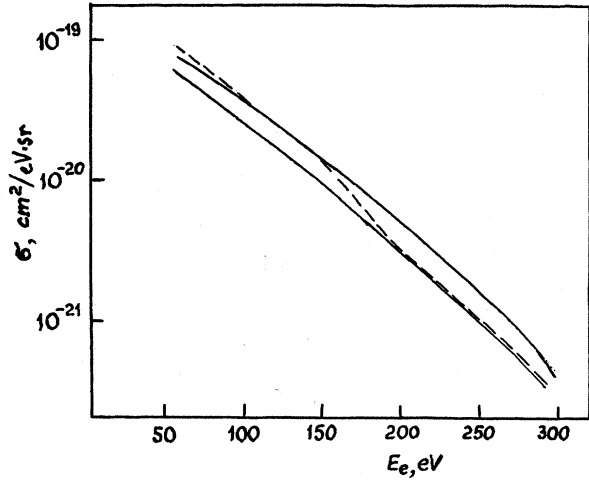


FIG. 16. Continuous part of energy spectra of electrons ejected in  $\text{Ar}^+-\text{Ar}$  collisions at the ion energy 100 keV. Broken line, experiment (RJV66); solid line, statistical calculations (BVS0-70). The lower theoretical curve is obtained taking into account the fraction of excitation energy carried away by fast Auger electrons.

doubly charged ion, then the transition probability should be twice as high. In the case of neutral atoms in the ground state the transition is impossible.

This theoretical prediction was checked experimentally for collisions  $\text{Ar}^{n+}-\text{Ar}$  (OFA69c) and  $\text{Ne}^{n+}-\text{Ne}$  (CKHE68) by studying the dependence of the relative yield of electrons ejected in  $L_1-MM$  transitions in argon and  $K-LL$  transitions in neon on the incident ion charge. It was found that the relative yield of electrons for doubly charged ions was indeed twice as high as that for singly charged ions. However, it proved that

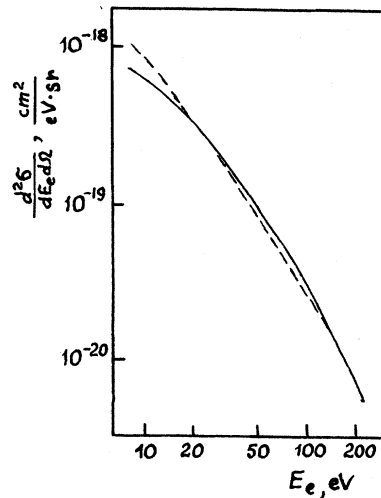


FIG. 17. Continuous part of energy spectra of electrons ejected in  $\text{Ar}^+-\text{Ar}$  collisions at the ion energy 15 keV. Broken line, experiment (OFA68); solid line, statistical calculations (O71).

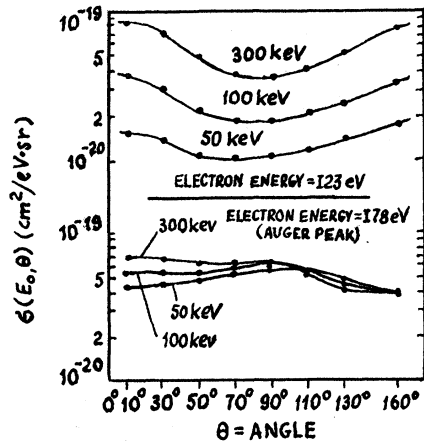


FIG. 18. Angular distribution of electrons ejected in  $\text{Ar}^+\text{-Ar}$  collisions (CJ70). The top curves are characteristic of the continuum electrons. The bottom curves are characteristic of the Auger electrons. The values of the incident ion energy are marked in the figure.

the yield for  $\text{Ne}^0\text{-Ne}$  was about 0.6 of that for  $\text{Ne}^+\text{-Ne}$  rather than zero (CKHE68). The reason for this discrepancy may be connected with the presence of highly excited ions in the primary beam and the transitions between orbitals in which two or more electrons are involved.

Cross sections for  $L_1$  argon and  $K$  neon excitation (curves 2 and 3 in Fig. 15) fit a linear dependence on ion velocity. Such a dependence was obtained theoretically by Bates and Williams (BW64) for  $2p\sigma\text{-}2p\pi$  transitions in the  $\text{H}^+\text{-H}$  system. However, the straight lines in Fig. 15 appear to cross the abscissa at a certain velocity rather than at  $v=0$  as in (BW64). It should be noted that the proton trajectory was considered in (BW64) as rectilinear even at small impact energies.

The formation of the continuous part of the electron energy spectrum in the collisions between two many-electron atomic systems is of rather complicated nature. Therefore, the only possible method for a theoretical description of experimental results is the use of statistical models. Such calculations were made in (BVSO70; O71) for  $\text{Ar}^+\text{-Ar}$  collisions. In the first of these works, Russek's model was used; in the other Firsov's model was used. Comparison between the calculations and the experimental results (OFAF 68; RJV66) is given in Figs. 16 and 17. Agreement of the data is quite reasonable. Thus it seems that the use of statistical models in calculations of energy spectra of electrons ejected in collisions between heavy atomic particles is promising enough. It should be noted that statistical calculations give lowered values of cross sections at low energies of ejected electrons. This fact may come from the assumption (F59; RM70) that the removal of electrons occurs after the collision. In practice, ionization can occur also

in a quasimolecule before departure of the colliding particles. This process requires less energy for electrons to be removed and can make a contribution to the low-energy region of the spectrum.

The angular distribution of electrons ejected in  $\text{Ar}^+\text{-Ar}$  collisions is given in Fig. 18. The distribution of the continuum electrons is not so strongly dependent on the ejection angle as in the case of  $\text{H}^+\text{-Ar}$ . Another difference is a noticeable backward emission of electrons observed in  $\text{Ar}^+\text{-Ar}$  collisions. The angular distribution of Auger electrons is nearly isotropic. The shape of the angular distribution is the least understood of the questions discussed in this section.

## CONCLUSIONS

The investigation of electron energy spectra represents a branch of physics of atomic collisions which is only beginning to develop. Therefore, in spite of noticeable progress made in recent years, the body of unsolved problems is still considerable. Especially great difficulties are faced in studying collisions between heavy atomic particles. It seems that the experimental study of electron energy spectra in the nearest future will be aimed at accumulating experimental data and improving experimental technique, including the use of coincidence technique. It seems important that these investigations be carried out in close contact with the study of inelastic energy losses and optical and x-ray emission. It is the united efforts of scientists working in these fields that may lead to the progress in studying the mechanism of inelastic atomic collisions.

## ACKNOWLEDGMENTS

The author is indebted to Professor V. M. Dukelsky, Professor V. V. Afrosimov, and Doctor Yu. S. Gordeev for helpful discussions and valuable advice.

- |        |  |
|--------|--|
| A65    | W. N. Asaad, Nucl. Phys. <b>66</b> , 494 (1965).   |
| AGPF64 | V. V. Afrosimov, Yu. S. Gordeev, M. N. Panov, and N. V. Fedorenko, Zh. Tech. Fiz. <b>34</b> , 1613 (1964).     |
| AlMo66 | P. L. Altick and E. N. Moore, Phys. Rev. <b>147</b> , 59 (1966).   |
| AM68   | W. N. Asaad and W. Mehlhorn, Z. Phys. <b>217</b> , 304 (1968).   |
| B61    | H. W. Berry, Phys. Rev. <b>121</b> , 1714 (1961).  |
| B62    | H. W. Berry, Phys. Rev. <b>127</b> , 1634 (1962).  |
| BB66   | R. B. Barker and H. W. Berry, Phys. Rev. <b>151</b> , 14 (1966).   |
| BBA69  | J. Baudon, M. Barat, and M. Abignoli, J. Phys. <b>B1</b> , 1083 (1969).  |
| BDO57  | D. R. Bates, M. R. C. McDowell, and A. Omholt, J. Atmospheric Terrest. Phys. <b>10</b> , 51 (1957).            |
| Be33   | H. A. Bethe, "Handbuch der Physik" (Springer, Berlin, 1933) Vol 24/1, p. 273.                                  |
| BG53   | D. R. Bates and G. Griffing, Proc. Phys. Soc. <b>A66</b> , 961 (1953).   |
| BGKS68 | V. V. Balashov, S. I. Grishanova, I. M. Kruglova, and V. S. Senashenko, Phys. Letters <b>27A</b> , 101 (1968). |
| BI57   | E. Blauth, Z. Phys. <b>147</b> , 228 (1957).   |

- BMVS63 P. G. Burke, D. McVicar, and K. Smith, *Phys. Rev. Letters* **11**, 559 (1963).
- BuMcV65 P. G. Burke and D. McVicar, *Proc. Phys. Soc.* **86**, 989 (1965).
- BV70 T. F. M. Bensen and L. Vriens, *Physica* **47**, 307 (1970).
- BVSO70 D. J. Bierman, W. F. Van der Weg, C. Snoek, and D. Onderdelinden, *Physica* **46**, 244 (1970).
- BW64 D. R. Bates and D. A. Williams, *Proc. Phys. Soc.* **83**, 425 (1964).
- C61 E. J. Callan, *Phys. Rev.* **124**, 793 (1961).
- CJ70 R. K. Cacak and T. Jorgensen, Jr., *Phys. Rev.* **A2**, 1322 (1970).
- CKHE68 M. P. McCaughey, E. J. Knystautas, H. C. Hayden, and E. Everhart, *Phys. Rev. Letters* **21**, 65 (1968).
- CKR70 R. K. Cacak, Q. C. Kessel, and M. E. Rudd, *Phys. Rev.* **A2**, 1327 (1970).
- CR70 G. B. Crooks and M. E. Rudd, *Phys. Rev. Letters* **25**, 1599 (1970).
- DP61 M. R. C. McDowell and G. Peach, *Phys. Rev.* **121**, 1383 (1961).
- E54 G. A. Erskine, *Proc. Roy. Soc.* **A224**, 362 (1954).
- Ed67 A. K. Edwards, Ph.D. Thesis, University of Nebraska, Lincoln, Nebraska, 1967.
- EK65 E. Everhart and Q. C. Kessel, *Phys. Rev. Letters* **14**, 247 (1965).
- ER68 A. K. Edwards and M. E. Rudd, *Phys. Rev.* **170**, 140 (1968).
- F59 O. B. Firsov, *Zh. Eksp. Teor. Fiz.* **36**, 1517 (1959).
- Fa60 L. D. Faddeev, *Zh. Eksp. Teor. Fiz.* **39**, 1459 (1960).
- FL65 U. Fano and W. Lichten, *Phys. Rev. Letters* **14**, 627 (1965).
- G59 M. Gryzinski, *Phys. Rev.* **115**, 374 (1959).
- G65 M. Gryzinski, *Phys. Rev.* **138A**, 322 (1965).
- GK61 S. S. Gershtein and V. D. Krivchenkov, *Zh. Eksp. Teor. Fiz.* **40**, 1491 (1961).
- GO71 Yu. S. Gordeev and G. N. Ogurtsov, *Zh. Eksp. Teor. Fiz.* **60**, 2051 (1971).
- KJ63 C. E. Kuyatt and T. Jorgensen, Jr., *Phys. Rev.* **130**, 1444 (1963).
- KP67 L. M. Kishinevsky and E. S. Parilis, *Proc. Intern. Conf. Phys. Electron. At. Collisions* 5th, 100 (1967).
- KSLCM70 M. O. Krause, F. A. Stevie, L. J. Lewis, T. A. Carlson, and W. E. Moddeman, *Phys. Letters* **31A**, 81 (1970).
- L63 W. Lichten, *Phys. Rev.* **131**, 229 (1963).
- L67 W. Lichten, *Phys. Rev.* **164**, 131 (1967).
- M67 W. Mehlhorn, *Z. Phys.* **208**, 1 (1967).
- Ma70 J. Macek, *Phys. Rev.* **A1**, 235 (1970).
- Mc65 R. P. Madden and K. Codling, *Astrophys. J.* **141**, 364 (1965).
- MEC69 R. P. Madden, D. L. Ederer and K. Codling, *Phys. Rev.* **177**, 136 (1969).
- MP58 D. E. Moe and O. H. Petsch, *Phys. Rev.* **110**, 1358 (1958).
- MP59 D. E. Moe and O. H. Petsch, *Phys. Rev.* **115**, 349 (1959).
- MS29 P. M. Morse and E. C. G. Stuckelberg, *Phys. Rev.* **33**, 932 (1929).
- MS68 W. Mehlhorn and D. Stalherm, *Z. Phys.* **217**, 294 (1968).
- O71 G. N. Ogurtsov, *Proc. Intern. Conf. Phys. Electron. At. Collisions* 7th, 100 (1971).
- OFAF68 G. N. Ogurtsov, I. P. Flaks, S. V. Avakyan, and N. V. Fedorenko, *Zh. Eksp. i Teor. Fiz., Pisma v Red.* **8**, 541 (1968).
- OFA69-a G. N. Ogurtsov, I. P. Flaks, and S. V. Avakyan, *Zh. Eksp. i Teor. Fiz.* **57**, 27 (1969).
- OFA69-b G. N. Ogurtsov, I. P. Flaks, and S. V. Avakyan, *Zh. Tech. Fiz.* **39**, 1293 (1969).
- OFA69-c G. N. Ogurtsov, I. P. Flaks, and S. V. Avakyan, *Proc. Intern. Conf. Phys. Electron. At. Collisions* 6th, 274 (1969).
- OFA70 G. N. Ogurtsov, I. P. Flaks, and S. V. Avakyan, *Zh. Tech. Fiz.* **40**, 2124 (1970).
- RG69 M. E. Rudd and D. Gregoire, "Physics of One- and Two-Electron Atoms", (North-Holland, 1969), p. 795.
- RJV66 M. E. Rudd, T. Jorgensen, Jr., and D. J. Volz, *Phys. Rev.* **151**, 28 (1966).
- RM70 A. Russek and J. Meli, *Physica* **46**, 222 (1970).
- RR37 E. G. Ramberg and F. K. Richtmyer, *Phys. Rev.* **51**, 913 (1937).
- RS55 R. A. Rubenstein and J. N. Snyder, *Phys. Rev.* **97**, 1653 (1955).
- RSB66 M. E. Rudd, C. A. Sauter, and C. L. Bailey, *Phys. Rev.* **151**, 20 (1966).
- RT58 A. Russek and M. T. Thomas, *Phys. Rev.* **109**, 2015 (1958).
- S63 J. A. R. Samson, *Phys. Rev.* **132**, 2122 (1963).
- Sa69 A. Salin, *J. Phys.* **B2**, 631 (1969).
- Sm67 B. M. Smirnov, *Zh. Eksp. Teor. Fiz.* **53**, 1400 (1967).
- TLE70 G. M. Thomson, P. C. Laudieri, and E. Everhart, *Phys. Rev.* **A1**, 1439 (1970).
- V68 D. J. Volz, Ph.D. Thesis, University of Nebraska, Lincoln, Nebraska (1968).
- VR70 D. J. Volz and M. E. Rudd, *Phys. Rev.* **A2**, 1395 (1970).